

# Structural, Biochemical, and Biophysical Characterization of Idelalisib Binding to Phosphoinositide 3-Kinase $\delta^*$

Received for publication, December 22, 2014, and in revised form, January 12, 2015. Published, JBC Papers in Press, January 28, 2015, DOI 10.1074/jbc.M114.634683

John R. Somoza<sup>†1</sup>, David Koditek<sup>§</sup>, Armando G. Villaseñor<sup>‡</sup>, Nikolai Novikov<sup>§</sup>, Melanie H. Wong<sup>§</sup>, Albert Licican<sup>§</sup>, Weimei Xing<sup>§</sup>, Leanna Lagpacan<sup>§</sup>, Ruth Wang<sup>§</sup>, Brian E. Schultz<sup>§</sup>, Giuseppe A. Papalia<sup>§</sup>, Dharmaraj Samuel<sup>§</sup>, Latesh Lad<sup>§</sup>, and Mary E. McGrath<sup>‡</sup>

From the Departments of <sup>†</sup>Structural Chemistry and <sup>§</sup>Biology, Gilead Sciences, Inc., Foster City, California 94404

**Background:** Idelalisib is a PI3K $\delta$  inhibitor used to treat hematological malignancies.

**Results:** Idelalisib is selective, noncovalent, reversible, and ATP-competitive.

**Conclusion:** The crystal structure helps explain the potency and selectivity of idelalisib. The biophysical and biochemical data clarify the details of the inhibitor's interactions with PI3K $\delta$ .

**Significance:** Its use in humans makes it important to understand how idelalisib inhibits PI3K $\delta$ .

Idelalisib (also known as GS-1101, CAL-101, IC489666, and Zydelig) is a PI3K $\delta$  inhibitor that has recently been approved for the treatment of several hematological malignancies. Given its use in human diseases, we needed a clear picture of how idelalisib binds to and inhibits PI3K $\delta$ . Our data show that idelalisib is a potent and selective inhibitor of the kinase activity of PI3K $\delta$ . A kinetic characterization clearly demonstrated ATP-competitive inhibition, and several additional biochemical and biophysical assays showed that the compound binds reversibly and noncovalently to the kinase. A crystal structure of idelalisib bound to the p110 $\delta$  subunit of PI3K $\delta$  furthers our understanding of the binding interactions that confer the potency and selectivity of idelalisib.

Class I PI3Ks catalyze the intracellular conversion of phosphatidylinositol 4,5-bisphosphate (PIP<sub>2</sub>)<sup>2</sup> to phosphatidylinositol 3,4,5-trisphosphate (PIP<sub>3</sub>), which functions as a second messenger, recruiting and activating signaling proteins such as Akt. Signals are relayed from receptor tyrosine kinases and G protein-coupled receptors to pathways regulating metabolism, cell growth and proliferation, motility, and differentiation.

PI3K $\delta$  is a class I PI3K that is formed by a catalytic subunit (p110 $\delta$ ) and a regulatory subunit (p85). The observation that PI3K $\delta$  is selectively expressed in leukocytes suggested that this isoform might be a therapeutic target for diseases in which

there is pathological activation of the Akt pathway in hematopoietic cells. Hematological malignancies of B cells, including indolent non-Hodgkin lymphoma, chronic lymphocytic leukemia, and mantle cell lymphoma, have constitutively active PI3K/Akt signaling pathways and respond to pathway inhibition (1–4).

Aberrant signaling in B cells is also found in a number of inflammatory diseases. PI3K $\delta$  inhibition interferes with B cell activation, survival, and migration (5). In rheumatoid arthritis, PI3K $\delta$  is highly expressed in the rheumatoid arthritis synovium (6) and in fibroblast-like synoviocytes, macrophages, and Th1 and Th17 cells (7). PI3K $\delta$  inhibition can modulate both B cell and T cell production of inflammatory cytokines. In models of rheumatoid arthritis, PI3K $\delta$  inhibitors have reduced inflammation and decreased bone and cartilage erosion (8).

Additional inflammatory diseases may benefit from blocking PI3K $\delta$  activity. Excessive PI3K $\delta$  activity in mast cells (9), neutrophils (10), T cells (11), eosinophils, and B cells contributes to the pathogenesis of allergic asthma. In a mouse model of asthma, PI3K $\delta$  inhibition attenuated airway hyper-responsiveness; decreased the influx of neutrophils, eosinophils, and lymphocytes to airways; and reduced IL-17 production (12).

Idelalisib is a potent and selective inhibitor of the kinase activity of PI3K $\delta$  (Fig. 1). The efficacy of this compound has been demonstrated in a series of human clinical studies (13–17), which led to the recent approval of Zydelig (idelalisib) in the United States and European Union. In the United States, Zydelig is indicated, in combination with rituximab, for the treatment of patients with relapsed chronic lymphocytic leukemia and as a monotherapy for patients with relapsed follicular B cell non-Hodgkin lymphoma and relapsed small lymphocytic lymphoma (18). In the European Union, Zydelig is indicated, in combination with rituximab, for the treatment of patients with relapsed chronic lymphocytic leukemia and refractory follicular B cell non-Hodgkin lymphoma and as first line therapy in chronic lymphocytic leukemia patients with 17p deletion or TP53 mutation who are unsuitable for chemoimmunotherapy (19). In this study, we describe the results of a set of biochemical and biophysical experiments aimed at defining how idelalisib inhibits PI3K $\delta$ .

\* This work was supported in part by funds from National Institutes of Health, National Institute of General Medical Sciences, and the Howard Hughes Medical Institute (to the Berkeley Center for Structural Biology) and by Contract DE-AC02-05CH11231 from the Director of the Office of Science, Office of Basic Energy Sciences, U.S. Department of Energy (to the Advanced Light Source).

⌘ Author's Choice—Final version full access.

The atomic coordinates and structure factors (code 4XE0) have been deposited in the Protein Data Bank (<http://www.pdb.org/>).

<sup>1</sup> To whom correspondence should be addressed: Gilead Sciences, Inc., 333 Lakeside Dr., Foster City, CA 94404. Tel.: 650-522-1624; E-mail: john.somoza@gilead.com.

<sup>2</sup> The abbreviations used are: PIP<sub>2</sub>, phosphatidylinositol 4,5-bisphosphate; PIP<sub>3</sub>, phosphatidylinositol 3,4,5-trisphosphate; Ni-NTA, nickel-nitrilotriacetic acid; ABD, adaptor-binding domain; bis-tris, 2-[bis(2-hydroxyethyl)amino]-2-(hydroxymethyl)propane-1,3-diol; TCEP, tris(2-carboxyethyl)phosphine hydrochloride.

## The Characterization of Idelalisib Binding to PI3K $\delta$

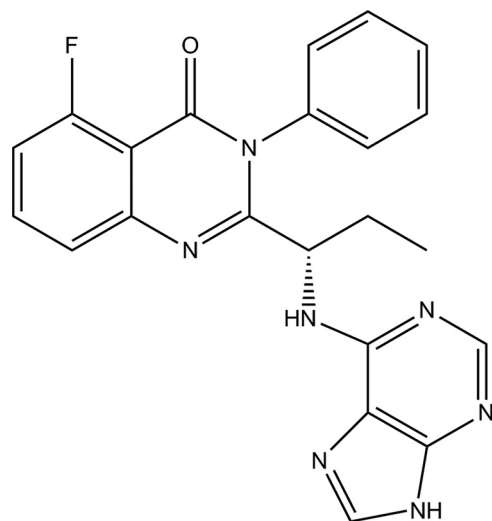


FIGURE 1. The structure of idelalisib (5-fluoro-3-phenyl-2-[(1S)-1-(9H-purin-6-ylamino)propyl]quinazolin-4(3H)-one).

### EXPERIMENTAL PROCEDURES

**Protein Expression and Purification**—The human p110 $\alpha$  and murine p110 $\delta$  catalytic subunits were co-expressed with the p85 $\alpha$  regulatory subunit and purified as heterodimers. Human p110 $\gamma$  was expressed and purified without a regulatory subunit. PI3K $\beta$  was purchased from Millipore (Billerica, MA) (item 14-603, lot 1994929-B).

Polyhistidine tags engineered at the N termini of the p110 constructs were used to purify the protein. The p110 domains and p85 $\alpha$  were cloned into *pFastBacHTa* and *pFastBac* dual vectors, respectively. *Spodoptera frugiperda* (*Sf21*) cells at a density of  $1.5 \times 10^6$  cells/ml were infected with an optimized ratio of viruses for 70 h at 27 °C. 20 g of cell pellets were processed for each of these samples, and the protein was purified using a Ni-NTA FF column (GE Life Sciences) and was buffer-exchanged using a KW2003 SEC column (Showa Denko America, New York, NY). The final sample of p110 $\alpha$ -p85 $\alpha$  was delivered in 20 mM HEPES (pH 7.5), 150 mM NaCl, and 1 mM DTT. P110 $\delta$ -p85 $\alpha$  was delivered in 25 mM HEPES (pH 7.5), 40% glycerol, 300 mM NaCl, and 3 mM CHAPS. P110 $\gamma$  was delivered in 25 mM HEPES (pH 7.5), 10% glycerol, 200 mM NaCl, and 2 mM DTT.

A second p110 $\delta$  construct was prepared with an rTEV-digestible site inserted after the adaptor-binding domain (ABD) and co-expressed with the iSH2 domain of p85 $\alpha$ . The cloning, expression, and purification strategies for this construct were adapted from a published protocol (20). The addition of 3 mM CHAPS to the lysis buffer helped maximize the recovery of the p110 $\delta$ /iSH2-p85 $\alpha$  complex from the cell pellet. Cell lysate after clarification was loaded on a Ni-NTA FF column and extensively washed with lysis buffer (20 CV) containing 1 M NaCl to remove contaminant proteins. The pure heterodimer was eluted from the column and digested with the rTEV protease to remove the iSH2 and ABD domains. The resulting protein was passed through a Ni-NTA FF column, and the flow-through portion containing  $\Delta$ ABD-p110 $\delta$  protein was pooled, concentrated, and loaded onto a size exclusion chromatography column (KW2003) pre-equilibrated with a buffer containing 20

mM Tris-HCl (pH 7.2), 50 mM (NH<sub>4</sub>)<sub>2</sub>SO<sub>4</sub>, 1% (v/v) ethylene glycol, 1% (w/v) betaine, 300 mM CHAPS, and 5 mM tris(2-carboxyethyl)phosphine hydrochloride (TCEP). Fractions containing the protein of interest were pooled and concentrated to 20 mg/ml for crystallization trials. The final sample had 15% polydispersity as measured by dynamic light scattering (Wyatt Technology, Santa Barbara, CA), and the purity was 98% as determined by SDS-PAGE analysis.

**Enzymatic Activity of the Class I PI3K Isoforms**—We measured IC<sub>50</sub> values for all four class I PI3Ks. The full-length protein used for the PI3K $\alpha$ ,  $\gamma$ , and  $\delta$  measurements is described above. The PI3K $\beta$  consisted of a complex of N-terminal His<sub>6</sub>-tagged recombinant full-length human p110 $\beta$  and untagged, full-length, human p85 $\alpha$  (Millipore).

The enzymatic activity of the class I PI3K isoforms was measured using a time-resolved FRET assay that monitors formation of the product PIP<sub>3</sub>, because it competes with fluorescently labeled PIP<sub>3</sub> for binding to the GRP-1 pleckstrin homology domain protein. An increase in PIP<sub>3</sub> product results in a decrease in time-resolved FRET signal as the labeled fluorophore is displaced from the GRP-1. PI3K isoforms were assayed under initial rate conditions in the presence of 25 mM HEPES (pH 7.4), and  $2 \times K_m$  ATP (100–300  $\mu$ M), 10  $\mu$ M PIP<sub>2</sub>, 5% glycerol, 5 mM MgCl<sub>2</sub>, 50 mM NaCl, 0.05% (v/v) CHAPS, 1 mM dithiothreitol, 1% (v/v) DMSO at the following concentrations for each isoform: PI3K $\alpha$ ,  $\beta$ ,  $\delta$  at 25–50  $\mu$ M and PI3K $\gamma$  at 2 nM. After an assay reaction time of 30 min at 25 °C, reactions were terminated with a final concentration of 10 mM EDTA, 10 nM labeled PIP<sub>3</sub>, and 35 nM europium-labeled GRP-1 detector protein before reading time-resolved FRET on an Envision plate reader (excitation, 340 nm; emission, 615/665 nm; delay, 100  $\mu$ s; and read window, 500  $\mu$ s). The data were normalized based on positive (1  $\mu$ M wortmannin) and negative (DMSO) controls, and IC<sub>50</sub> values were calculated from the fit of the dose-response curves to a four-parameter equation. All IC<sub>50</sub> values represent geometric mean values of a minimum of four determinations. These assays generally produced results within 3-fold of the reported mean. The KINOMEScan platform (DiscoverX, San Diego, CA) was used to assess the interaction of idelalisib, at a concentration of 10  $\mu$ M, with the ATP-binding site of a broad set of kinases (21).

**Competition of Idelalisib with ATP**—To solutions of recombinant PI3K $\delta$  (p110 $\delta$ -p85 $\alpha$ ) (final concentration, 15  $\mu$ M) in reaction buffer from the PI3K HTRF assay kit (Millipore) was added idelalisib at concentrations from 0 to 80 nM (final concentration). After a 1-h preincubation period, PIP<sub>2</sub> was added to a final concentration of 10  $\mu$ M, and ATP was added at concentrations from 0 to 1.5 mM to initiate the reaction. After 45 min, the reactions were quenched with a stop solution from the assay kit. A detection solution was then added to each well, and the mixture was further incubated for 2 h. Time-resolved fluorescence was measured with a Tecan Infinite M1000 plate reader, using an excitation wavelength of 330 nm and emission wavelengths of 620 and 665 nm. The ratio of emission at 665 nm to that at 620 nm was used as the measure of reaction rate. The rate data were fit globally using the equation  $v = V_{max} [S] / (K_m (1 + [I]/K_i) + [S](1 + [I]/\alpha K_i))$ , where  $v$  is the observed reaction rate,  $V_{max}$  is the maximum reaction rate,  $[S]$  is the concentra-

tion of ATP,  $K_m$  is the Michaelis constant for ATP,  $[I]$  is the concentration of idelalisib,  $K_i$  is the inhibition constant for idelalisib, and  $\alpha$  is a multiplier for  $K_i$  that describes the competition behavior. Values of  $\alpha \gg 1$  are indicative of competitive inhibition, values of  $\alpha$  approximately equal to 1 imply noncompetitive inhibition, and values of  $\alpha \ll 1$  are characteristic of uncompetitive inhibitors (22).

**Reversibility Assay**—Solutions of 3 nM PI3K $\delta$ -p 85 $\alpha$  were preincubated with either 400 nM idelalisib or 100 nM wortmannin for 1 h. One microliter of solution was transferred to 99  $\mu$ l of reaction buffer solution containing 10  $\mu$ M PIP2 and 300  $\mu$ M ATP to initiate the enzyme reaction. At 5-min intervals, samples from each reaction were quenched with HTRF stop solution, and fluorescence was measured using the detection kit as described above. The reactions were measured over a time frame of 40 min. Control reactions consisted of the reaction of 30 pM PI3K $\delta$  in the absence of inhibitor, the reaction of 30 pM PI3K $\delta$  in the presence of 400 nM idelalisib or 100 nM wortmannin, and the reaction of 30 pM PI3K $\delta$  in the presence of 4 nM idelalisib or 1 nM wortmannin. The data were analyzed with linear least square fits to obtain reaction rates.

**Surface Plasmon Resonance Binding Assay**— $\Delta$ ABD-p110 $\delta$  was minimally biotinylated using a 1:1 molar ratio of protein to EZ-link sulfo-NHS-LC-LC-biotin (ThermoScientific; catalog no. 21338). The binding site was protected from biotinylation by adding 10  $\mu$ M of idelalisib to 9  $\mu$ M of protein prior to addition of EZ-link sulfo-NHS-LC-LC-biotin. Biotinylation in the absence of idelalisib protection was also tested. Following incubation for 1 h at 4  $^{\circ}$ C, the mixture was desalted using a Zeba spin desalting column (ThermoScientific; catalog no. 89883) pre-equilibrated in Biacore running buffer (25 mM HEPES, pH 7.5, 150 mM NaCl, 5 mM MgCl $_2$ , 1 mM TCEP, 5% glycerol, 0.05% P20) to remove any unreacted biotin. The presence of one biotin molecule per protein molecule was confirmed by mass spectrometry. Characterization of inhibitor binding and dissociation was performed using a Biacore T100 instrument and research grade series S CM5 sensor chips (GE Healthcare; catalog no. BR-1005-30). Before use, CM5 sensor chips were pre-conditioned using two 6-s pulses each of 100 mM HCl, 50 mM NaOH, 0.5% (w/v) SDS, and deionized H $_2$ O at a flow rate of 100  $\mu$ l/min. Approximately 15,000 response units (RU) of neutravidin was immobilized on all four surfaces via standard amine-coupling chemistry (GE Healthcare; catalog no. BR-1000-50) in HBS-P buffer (10 mM HEPES, pH 7.4, 150 mM NaCl, 0.005% P20). Biotinylated protein was injected over separate flow cells to achieve capture levels ranging between 6,000 and 14,000 response units. Any remaining free sites on neutravidin were blocked with two 5-min pulses of 50  $\mu$ M EZ-Link-Amine-PEG $_2$ -Biotin (ThermoScientific; catalog no. 21346) at a flow rate of 30  $\mu$ l/min. Idelalisib at concentrations of 0.12, 0.37, 1.1, 3.3, 10, and 30 nM (in duplicate) was injected for a 90-s association time and a 1–200-s dissociation time at a flow rate of 100  $\mu$ l/min. Wortmannin was injected on a separate sensor chip at a concentration of 2  $\mu$ M for an 8-min association phase and a 1-hour dissociation phase. At the end of each injection cycle, the injection needle and tubing were washed with 50% DMSO using the “extra wash” command. A five-point DMSO concentration series (ranging from 0.8% to 1.2% DMSO) was included to gen-

**TABLE 1**  
Idelalisib potency and class I selectivity at  $[ATP] = 2 \times K_m$

	Time-resolved FRET ATP $K_m$	IC $_{50}$ at $2 \times$ $K_m$ ATP	IC $_{50}$ -based PI3K $\delta$ fold selectivity
	$\mu$ M	nM	
PI3K $\alpha$	48	8600	453
PI3K $\beta$	279	4000	210
PI3K $\delta$	118	19	1
PI3K $\gamma$	37	2100	110

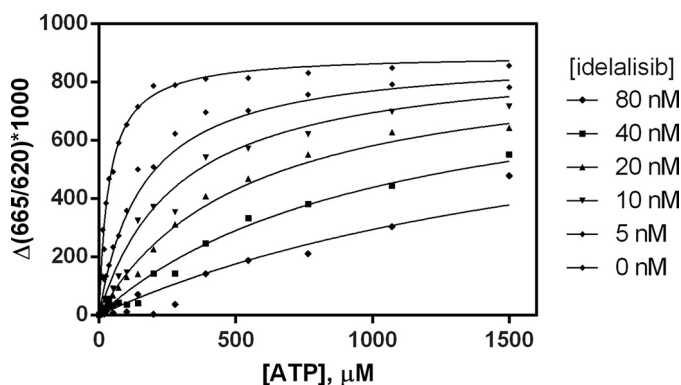


**FIGURE 2. Competition of idelalisib with ATP against PI3K $\delta$ .** Reaction rates were determined at various concentrations of ATP and idelalisib, and the data were fit globally with a general inhibition model to characterize the competitive behavior.

erate a calibration curve to correct for excluded volume effects. Sensorgrams were double-referenced and corrected for solvent effects using Scrubber 2.0c software (Biologic Software, Campbell, Australia) but fitted using both Scrubber and CLAMP software (23).

The data were fitted using a mass transport model (24, 25). Three independent surfaces were globally fit for the association and dissociation rates  $k_a$  and  $k_d$ , while floating the maximum binding response ( $R_{max}$ ) and mass transport ( $k_t$ ) constant for each surface. The solutions from the fits for all three surfaces from both Scrubber and CLAMP all showed  $k_a^*R_{max}/k_t$  values of  $< 5$  (a measure of the suitability of the solution to yield unique values for  $k_a$  and  $k_d$ ) (26). Additionally, kinetic values derived from the global fit using CLAMP software were not highly correlated. The observed correlation coefficients for  $k_a$  versus  $k_d$  were 0.62 and 0.67 in replicate experiments, demonstrating that although the sensorgrams are influenced by mass transport, a unique solution for these parameters can be determined (24, 25). Both fitting routines yielded values for  $k_a$  and  $k_d$  for identical surfaces that did not differ appreciably ( $< 4.5\%$ ). For wortmannin, only an off-rate analysis was performed.

**X-ray Crystallography**—Crystals used for seeding were obtained by vapor diffusion at 20  $^{\circ}$ C with 25 nl of 11 mg/ml  $\Delta$ ABD-p110 $\delta$  and 0.9 mM of a p110 $\delta$  inhibitor in protein storage buffer (20 mM Tris, pH 7.2, 50 mM (NH $_4$ ) $_2$ SO $_4$ , 1% v/v ethylene glycol, 1% (w/v) betaine, 0.3  $\mu$ M CHAPS, and 5 mM TCEP) added to 25 nl of reservoir solution (25% (w/v) PEG 3350, 0.1 M bis-tris (pH 6.5)). Crystals were pulverized, pooled together in the reservoir solution, vortexed with a Seed-Bead (Hampton Research) for 45 s, flash-frozen in liquid nitrogen, and stored at  $-80$   $^{\circ}$ C. For seeding crystallization trials, the frozen seed was thawed and diluted 500-fold in 25% (v/v) PEG 300, 0.1 M Tris (pH 8.5).

## The Characterization of Idelalisib Binding to PI3K $\delta$

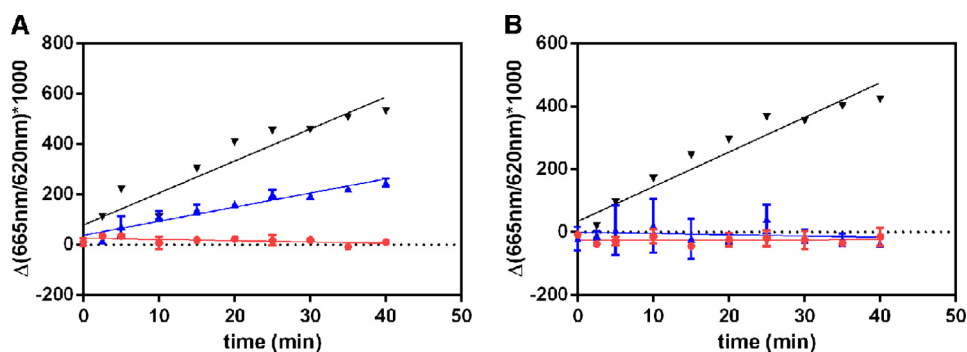


FIGURE 3. **Reversibility experiments with idelalisib (A) and wortmannin (B).** For each experiment, the progress curves are denoted as follows: *black*, DMSO (no inhibitor) enzyme control; *blue*, activity following 100-fold dilution of test compound preincubated with enzyme; and *red*, enzyme activity in the presence of 400 nM idelalisib or 100 nM wortmannin. The *red* progress curve gives the expected activity of the preformed enzyme-inhibitor complex if no compound dissociation occurs upon dilution.

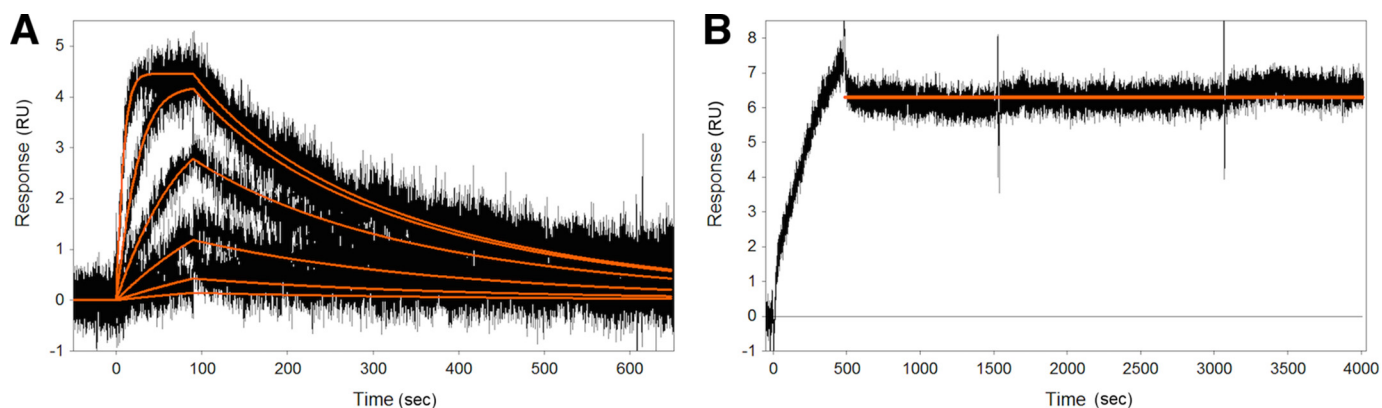


FIGURE 4. **Shown are sensorgrams from representative surfaces of neutravidin-captured p110 $\delta$  binding to idelalisib (A) and wortmannin (B).** Idelalisib was injected at concentrations of 0.12, 0.37, 1.1, 3.3, 10, and 30 nM (the latter being injected in duplicate). Wortmannin was injected at a concentration of 2  $\mu$ M. RU, response units.

Preparation of diffraction quality  $\Delta$ ABD-p110 $\delta$ :idelalisib crystals started with a mixture of 0.48  $\mu$ l of 2.5% (w/v) *n*-dodecyl- $\beta$ -D-maltoside, 0.30  $\mu$ l of 20 mM ligand, and 12  $\mu$ l of 12 mg/ml  $\Delta$ ABD-p110 $\delta$  in storage buffer (described above). The mixture was allowed to sit for 1 h at room temperature instead of 4  $^{\circ}$ C to prevent the formation of white precipitate. Seeded vapor diffusion droplets were assembled by adding 90 nl of the 500-fold diluted seed (described above) to 100 nl of the *n*-dodecyl- $\beta$ -D-maltoside-ligand- $\Delta$ ABD-p110 $\delta$  mixture. The droplets were equilibrated against reservoir wells containing 50  $\mu$ l of 1% to 30% (v/v) PEG 300, 0.1 M Tris (pH 8.5) at 20  $^{\circ}$ C. Crystals appeared in 2–5 days across the 1% to 30% PEG range. Crystals were cryoprotected in 20% (w/v) glycerol, 25% (w/v) PEG 300, 0.1 M Tris (pH 8.5), 50 mM ammonium sulfate, 0.2% (w/v) *n*-dodecyl- $\beta$ -D-maltoside, 0.2 mM ligand and were flash-frozen in liquid nitrogen for data collection.

Diffraction data were collected on Beamline 5.0.1 at the Advanced Light Source (Berkeley, CA). The data were reduced using Mosflm (27) and Aimless (28). The structure was solved by molecular replacement using EPMR (29) and refined using the Phenix software package (30), and the electron density was fit using Coot (31). The inhibitor and surrounding ATP-binding site are very clearly defined in the electron density maps. The coordinates as well as the diffraction data have been deposited in the Protein Data Bank under code 4XE0.

## RESULTS AND DISCUSSION

*In Vitro Potency and Selectivity*—Table 1 shows the idelalisib IC<sub>50</sub> values for each class I isoform measured in the presence of  $2 \times K_m$  ATP. The IC<sub>50</sub> of idelalisib for PI3K $\delta$  is 19 nM, whereas the IC<sub>50</sub> values for PI3K $\alpha$ , PI3K $\beta$ , and PI3K $\gamma$  are 8,600, 4,000, and 2,100 nM, respectively. Thus, idelalisib potently inhibits PI3K $\delta$  and is selective relative to the other class I isoforms (453-, 210-, and 110-fold selective against the  $\alpha$ ,  $\beta$ , and  $\gamma$  isoforms, respectively). Testing of a broad panel of 351 kinases and 44 mutant kinases (21) at 10  $\mu$ M idelalisib showed that the most potent inhibition seen for any non-PI3K kinase was a percent inhibition of 47%.

*Idelalisib Is an ATP-competitive Inhibitor*—The ability of idelalisib to compete with ATP binding to PI3K $\delta$  was tested in enzymatic assays. The activity of PI3K $\delta$  was measured at various concentrations of ATP and idelalisib, and the data were fit globally to the competition expression described under “Experimental Procedures.” The results are shown in Fig. 2. The global fit yielded the following kinetic parameters:  $K_m = 37 \pm 3 \mu$ M and  $K_i = 1.5 \pm 0.1$  nM. The measured  $K_m$  value of 37  $\mu$ M from the competition data was slightly lower than the value reported in Table 1, but this difference did not significantly affect the data analysis.

The fit for the parameter  $\alpha$  gave a very high value that reached the limits of the data fitting program. The high value

of  $\alpha$  ( $\alpha \gg 1$ ) demonstrates ATP-competitive inhibition by idelalisib. As confirmation of the ATP competition, a fit of the kinetic data with a pure competitive model gave identical values for  $K_m$  and  $K_i$  with the same goodness of fit (data not shown).

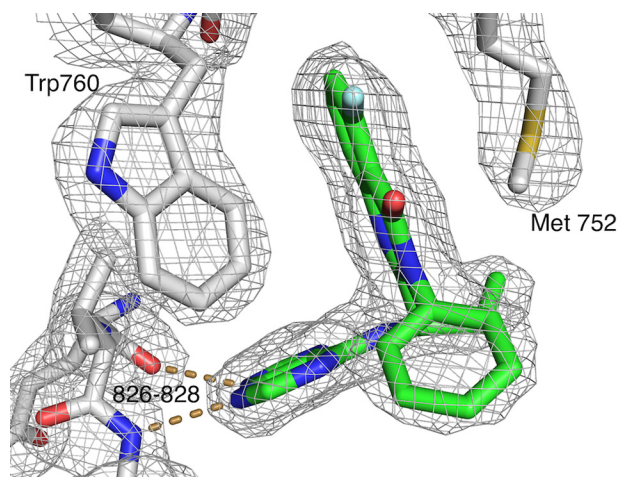


FIGURE 5. X-ray crystal structure of idelalisib bound in the PI3K $\delta$  ATP-binding site. The  $2F_o - F_c$  electron density is contoured at  $1.2 \sigma$ . The dashed lines represent hydrogen bonds to the hinge region of the kinase. For clarity, only a few residues are shown.

TABLE 2

## Data and refinement statistics

Data	
Space group	C2
Cell parameters (Å)	142.1, 64.6, 116.0, $\beta = 103.1^\circ$
Resolution range (last shell) (Å)	69.2–2.4 (2.5–2.4)
Number of observations	136,588
Number of unique reflections	38,471
Completeness (last shell) (%)	99.4 (98.8)
$\langle I \rangle / \langle \sigma(I) \rangle$ (last shell)	9.7 (2.7)
CC1/2 (last shell)	0.995 (0.77)
Average B-factor of the model (Å <sup>2</sup> )	41
Wilson B-factor (Å <sup>2</sup> )	36.0
Model	
Subunits in asymmetric unit	1
Number of water molecules	224
Resolution used for refinement (Å)	69.2–2.4
Sigma cutoff ( $F/\sigma(F)$ )	0.0
R-factor (last shell)	0.21 (0.24)
Free R (last shell)	0.29 (0.33)
Root mean square deviation from ideal geometry: bonds (Å)/angles ( $^\circ$ )	0.009/1.21
Ramachandran plot: favored/outliers (%)	94/1.5

*Idelalisib Is a Reversible Inhibitor*—Along with the kinetic characterization of idelalisib described above, two additional studies showed that it is a reversible inhibitor. Dilution experiments showed that the kinase can be completely inhibited with idelalisib at concentrations  $\sim 20$ -fold greater than its  $IC_{50}$ . However, enzyme activity was quickly recovered following a 1:100 dilution of the enzyme-inhibitor complex into a buffer solution containing the ATP and PIP<sub>2</sub> substrates. DMSO and the irreversible inhibitor wortmannin were used as control compounds (Fig. 3, A and B). The rate of PIP<sub>2</sub> phosphorylation upon dilution was approximately one-half of that of the DMSO control. This rate is consistent with the steady-state reaction rate of PI3K $\delta$  in the presence of 4 nM idelalisib. Because the reaction was sampled at 5-min intervals, no distinct kinetic phase for compound dissociation was observed. However, based on the linearity of the progress curve, the dissociation of inhibitor likely occurred within the first few minutes of reaction time. In contrast, enzyme preincubated with wortmannin did not show detectable recovery of activity upon dilution. The dilution of wortmannin-inhibited PI3K $\delta$  did not lead to an increased reaction rate, implying that no dissociation of wortmannin occurred during dilution and the subsequent enzymatic reaction. These results demonstrate that idelalisib is a reversible inhibitor of PI3K $\delta$ .

Surface plasmon resonance studies further confirmed the reversibility of idelalisib. The Biacore platform was used to examine the direct molecular interaction of idelalisib to biotinylated p110 $\delta$  captured on a neutravidin surface. Sensorgrams for idelalisib (Fig. 4A) showed a specific, saturable, dose-responsive interaction with p110 $\delta$ . Duplicate injections of the inhibitor at 30 nM on the same surface overlay well, demonstrating the stability of the captured protein. The maximum signal,  $R_{max}$ , was kept low at single-digit response units to minimize the influence of mass transport for this compound. Idelalisib binding is characterized by a very fast on rate,  $k_a = 5.18 \times 10^6 \text{ M}^{-1} \text{ s}^{-1}$ , and a moderate off rate,  $k_d = 6.34 \times 10^{-3} \text{ s}^{-1}$ . A replicate experiment yielded values that differed by 3 and 16% in  $k_a$  and  $k_d$ , respectively. More importantly, the response signal during the dissociation phase returned to baseline level for idelalisib, indicating complete dissociation of the compound from the protein. The wortmannin control (Fig. 4B) showed no dissociation after 1 h, consistent with this compound binding

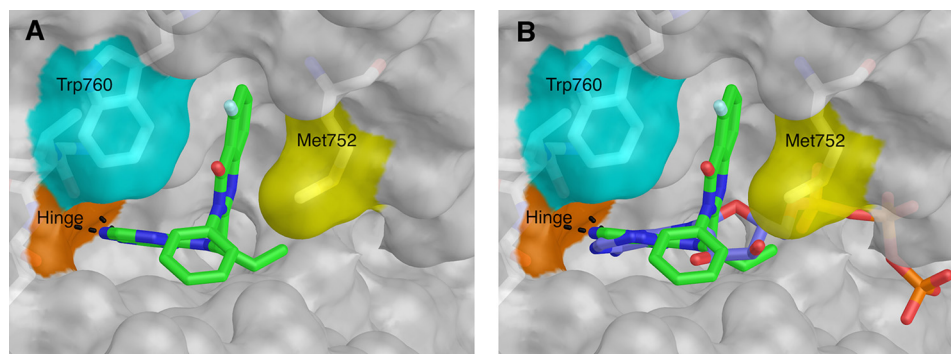


FIGURE 6. A, structure of idelalisib (green) bound to the PI3K $\delta$  ATP-binding site. Met-752 (yellow) and Trp-760 (cyan) form the sides of the specificity pocket. The hinge region is shown in orange, and hydrogen bonds between the inhibitor and the hinge are shown as dashed lines. B, idelalisib (green) bound to PI3K $\delta$ . The ATP was placed in the PI3K $\delta$  binding site by superimposing (using the “align” command in PyMOL) the structure of PI3K $\gamma$  bound with ATP (accession code 1E8X) (35).

## The Characterization of Idelalisib Binding to PI3K $\delta$

irreversibly to p110 $\delta$  (32). No nonspecific binding of idelalisib and wortmannin on the neutravidin reference surface was observed (data not shown). Biotinylation without idelalisib protection did not affect the results (data not shown). The reversibility of idelalisib may have implications for drug safety; some irreversible inhibitors may be more susceptible to off-target binding or have a slightly increased risk of idiopathic toxicity compared with reversible inhibitors (33).

**Crystal Structure of PI3K $\delta$  in Complex with Idelalisib**—We determined the crystal structure of  $\Delta$ ABD-p110 $\delta$  in the presence of idelalisib (Fig. 5) (Protein Data Bank code 4XE0). The data and refinement statistics are summarized in Table 2.

The protein used for crystallography was comprised of 939 residues, of which 815 were observed in the electron density. Aside from the missing residues, a significant fraction of the protein has weak electron density and correspondingly high temperature factors. The kinase domain and, in particular the ATP-binding site, is well defined by the electron density, but the Ras-binding and C2 domains have higher temperature factors and are more mobile, as are the residues that link the ABD and the Ras-binding domain. The C-terminal end of the helical domain (roughly residues 630–675) interacts with residues from both the N- and C-terminal lobes of the kinase. This section shows relatively low temperature factors, whereas the rest

of the helical domain is more mobile. It seems likely that the more mobile parts of the protein would be stabilized when interacting with the ABD, the p85 subunit, and with additional binding partners in the cell.

Idelalisib binds in the ATP-binding pocket (Fig. 6, A and B). When compared with the binding of ATP, the inhibitor forms hydrogen bonds to the hinge region that are very similar to those made by ATP (Fig. 6B). However, the remaining interactions with the protein are very different from what are seen for ATP binding (Fig. 6B).

Idelalisib is a propeller-shaped inhibitor and adopts a binding mode similar to what was described for the binding of another propeller-shaped inhibitor: IC87114 (20, 34). The electron density for idelalisib shows that there is no covalent bond between the inhibitor and the protein. This is in contrast, for example, with the electron density of wortmannin bound to PI3K $\gamma$ , where there is clear density for the covalent bond with Lys-833 (35).

The purine group of idelalisib serves as the hinge binder, with hydrogen bonds between the purine N3 and the backbone amide of Val-828 and between N9 and the backbone carbonyl oxygen of Glu-826 (Fig. 7). The purine N7 forms part of a water-mediated hydrogen bond network that includes N1 of the quinazolinone and the side chain of Asp-911 (Fig. 7). The ethyl group of the inhibitor binds in a hydrophobic pocket formed by Ile-910, Met-900, and Met-752.

A comparison of the idelalisib-bound and apo structures (Protein Data Bank code 1EAX) shows that the ATP-binding site requires a substantial conformational change to accommodate idelalisib (Fig. 8, A and B). In the apo enzyme, Met-752 and Trp-760 are packed against each other, but in the presence of idelalisib these two residues lie  $\sim 6.5$  Å apart, opening a hydrophobic pocket (the specificity pocket) in which the fluoro-quinazolinone of the inhibitor binds (Fig. 8, A and B). Similar to what was seen previously, the plane of the quinazolinone ring system is parallel to the sides of the pocket, displaying a hydrophobic interaction with the kinase (20).

The phenyl moiety of idelalisib packs against the side chains of Asp-832, Thr-833, and Asn-836. Our SAR data<sup>3</sup> and the work of Cushing *et al.* (36) on another propeller-shaped series suggest that modifications at this position affect the potency and selectivity across the PI3K class I family.

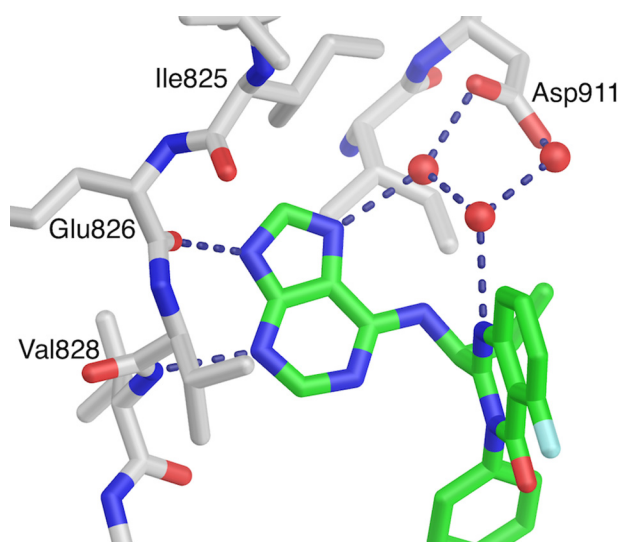


FIGURE 7. Water-mediated hydrogen bonds between the p110 $\delta$  and idelalisib. To expose the inhibitor, much of the protein is not shown.

<sup>3</sup> Manuscript in preparation.

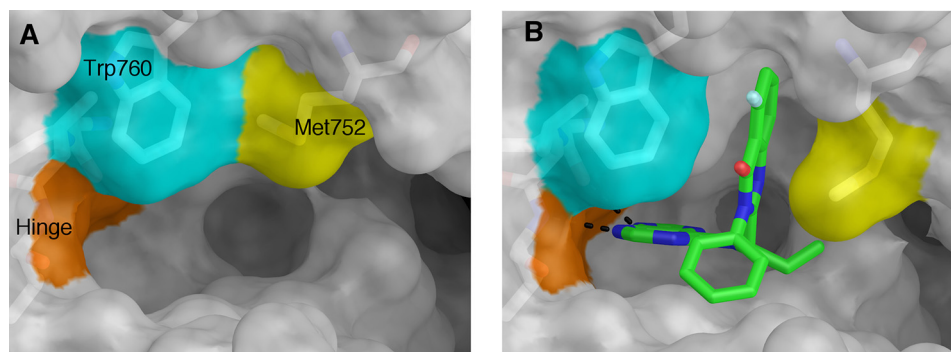


FIGURE 8. Comparison of apo PI3K $\delta$  (Protein Data Bank accession code 2WXR) (A) and idelalisib-bound PI3K $\delta$  showing the opening of the specificity pocket that accompanies idelalisib binding (B).

The p110 $\delta$  side chains that interact with idelalisib are conserved across the class I isoforms. However, the opening of the specificity pocket requires conformational changes in areas further from the ATP-binding site that no longer share sequence identity across the family. Knight *et al.* (37) studied the binding of PI3K $\gamma$  to another propeller-shaped inhibitor (PIK-39) and made the argument that the selectivity of the propeller-shaped inhibitors is at least partially a reflection of how much energy it takes to open the specificity pocket in each isoform. Berndt *et al.* (20) came to the same conclusion based on their structural and modeling work on IC87114 binding to PI3K $\delta$ . IC87114 has a purine hinge binder and accesses the specificity pocket with a quinazolinone. Overall, these observations support the idea that engagement of the specificity pocket upon kinase binding contributes to the selectivity profile of idelalisib.

**Conclusions**—Our *in vitro* biochemical data showed that idelalisib potently and selectively inhibits the kinase activity of PI3K $\delta$ , and the kinetic characterization of inhibition demonstrated that it is competitive with ATP. The kinetic analysis, along with the dilution and surface plasmon resonance experiments, clearly showed that idelalisib binds reversibly to the enzyme.

The 2.4 Å crystal structure of the idelalisib-PI3K $\delta$  complex showed the inhibitor binding in the ATP-binding site and revealed the specific and entirely noncovalent interactions between inhibitor and protein. Idelalisib binds so as to open and occupy the specificity pocket, as seen for other propeller-shaped inhibitors. More generally, the structure provides a framework for understanding the potency of idelalisib, as well as its selectivity for PI3K $\delta$  over the rest of the class I PI3Ks and across the kinome.

**Acknowledgments**—We thank Prof. Roger Williams and Dr. Alex Berndt (Medical Research Council Laboratory of Molecular Biology) and Dr. Gary Phillips (Gilead Sciences) for helpful discussions. We also thank the Berkeley Center for Structural Biology at the Advanced Light Source (Berkeley, CA).

## REFERENCES

- Bernal, A., Pastore, R. D., Asgary, Z., Keller, S. A., Cesarman, E., Liou, H. C., and Schattner, E. J. (2001) Survival of leukemic B cells promoted by engagement of the antigen receptor. *Blood* **98**, 3050–3057
- Lannutti, B. J., Meadows, S. A., Herman, S. E., Kashishian, A., Steiner, B., Johnson, A. J., Byrd, J. C., Tyner, J. W., Loriaux, M. M., Deininger, M., Druker, B. J., Puri, K. D., Ulrich, R. G., and Giese, N. A. (2011) CAL-101, a p110 $\delta$  selective phosphatidylinositol-3-kinase inhibitor for the treatment of B-cell malignancies, inhibits PI3K signaling and cellular viability. *Blood* **117**, 591–594
- Hoellenriegel, J., Meadows, S. A., Sivina, M., Wierda, W. G., Kantarjian, H., Keating, M. J., Giese, N., O'Brien, S., Yu, A., Miller, L. L., Lannutti, B. J., and Burger, J. A. (2011) The phosphoinositide 3'-kinase  $\delta$  inhibitor, CAL-101, inhibits B-cell receptor signaling and chemokine networks in chronic lymphocytic leukemia. *Blood* **118**, 3603–3612
- Meadows, S. A., Vega, F., Kashishian, A., Johnson, D., Diehl, V., Miller, L. L., Younes, A., and Lannutti, B. J. (2012) PI3K $\delta$  inhibitor, GS-1101 (CAL-101), attenuates pathway signaling, induces apoptosis, and overcomes signals from the microenvironment in cellular models of Hodgkin lymphoma. *Blood* **119**, 1897–1900
- Bilancio, A., Okkenhaug, K., Camps, M., Emery, J. L., Ruckle, T., Rommel, C., and Vanhaesebroeck, B. (2006) Key role of the p110 $\delta$  isoform of PI3K in B-cell antigen and IL-4 receptor signaling: comparative analysis of genetic and pharmacologic interference with p110 $\delta$  function in B cells. *Blood* **107**, 642–650
- Bartok, B., Boyle, D. L., Liu, Y., Ren, P., Ball, S. T., Bugbee, W. D., Rommel, C., and Firestein, G. S. (2012) PI3 kinase  $\delta$  is a key regulator of synovioocyte function in rheumatoid arthritis. *Am. J. Pathol.* **180**, 1906–1916
- Firestein, G. S. (2004) The T cell cometh: interplay between adaptive immunity and cytokine networks in rheumatoid arthritis. *J. Clin. Invest.* **114**, 471–474
- Randis, T. M., Puri, K. D., Zhou, H., and Diacovo, T. G. (2008) Role of PI3K $\delta$  and PI3K $\gamma$  in inflammatory arthritis and tissue localization of neutrophils. *Eur. J. Immunol.* **38**, 1215–1224
- Ali, K., Bilancio, A., Thomas, M., Pearce, W., Gilfillan, A. M., Tkaczyk, C., Kuehn, N., Gray, A., Giddings, J., Peskett, E., Fox, R., Bruce, I., Walker, C., Sawyer, C., Okkenhaug, K., Finan, P., and Vanhaesebroeck, B. (2004) Essential role for the p110 $\delta$  phosphoinositide 3-kinase in the allergic response. *Nature* **431**, 1007–1011
- Puri, K. D., Doggett, T. A., Douangpanya, J., Hou, Y., Tino, W. T., Wilson, T., Graf, T., Clayton, E., Turner, M., Hayflick, J. S., and Diacovo, T. G. (2004) Mechanisms and implications of phosphoinositide 3-kinase  $\delta$  in promoting neutrophil trafficking into inflamed tissue. *Blood* **103**, 3448–3456
- Soond, D. R., Bjørgo, E., Moltu, K., Dale, V. Q., Patton, D. T., Torgersen, K. M., Galleway, F., Twomey, B., Clark, J., Gaston, J. S., Taskén, K., Bunyard, P., and Okkenhaug, K. (2010) PI3K p110 $\delta$  regulates T-cell cytokine production during primary and secondary immune responses in mice and humans. *Blood* **115**, 2203–2213
- Park, S. J., Lee, K. S., Kim, S. R., Min, K. H., Moon, H., Lee, M. H., Chung, C. R., Han, H. J., Puri, K. D., and Lee, Y. C. (2010) Phosphoinositide 3-kinase  $\delta$  inhibitor suppresses interleukin-17 expression in a murine asthma model. *Eur. Respir. J.* **36**, 1448–1459
- Brown, J. R., Byrd, J. C., Coutre, S. E., Benson, D. M., Flinn, I. W., Wagner-Johnston, N. D., Spurgeon, S. E., Kahl, B. S., Bello, C., Webb, H. K., Johnson, D. M., Peterman, S., Li, D., Jahn, T. M., Lannutti, B. J., Ulrich, R. G., Yu, A. S., Miller, L. L., and Furman, R. R. (2014) Idelalisib, an inhibitor of phosphatidylinositol 3-kinase p110 $\delta$ , for relapsed/refractory chronic lymphocytic leukemia. *Blood* **123**, 3390–3397
- Flinn, I. W., Kahl, B. S., Leonard, J. P., Furman, R. R., Brown, J. R., Byrd, J. C., Wagner-Johnston, N. D., Coutre, S. E., Benson, D. M., Peterman, S., Cho, Y., Webb, H. K., Johnson, D. M., Yu, A. S., Ulrich, R. G., Godfrey, W. R., Miller, L. L., and Spurgeon, S. E. (2014) Idelalisib, a selective inhibitor of phosphatidylinositol 3-kinase- $\delta$ , as therapy for previously treated indolent non-Hodgkin lymphoma. *Blood* **123**, 3406–3413
- Kahl, B. S., Spurgeon, S. E., Furman, R. R., Flinn, I. W., Coutre, S. E., Brown, J. R., Benson, D. M., Byrd, J. C., Peterman, S., Cho, Y., Yu, A., Godfrey, W. R., and Wagner-Johnston, N. D. (2014) A phase 1 study of the PI3K $\delta$  inhibitor idelalisib in patients with relapsed/refractory mantle cell lymphoma (MCL). *Blood* **123**, 3398–3405
- Gopal, A. K., Kahl, B. S., de Vos, S., Wagner-Johnston, N. D., Schuster, S. J., Jurczak, W. J., Flinn, I. W., Flowers, C. R., Martin, P., Viardot, A., Blum, K. A., Goy, A. H., Davies, A. J., Zinzani, P. L., Dreyling, M., Johnson, D., Miller, L. L., Holes, L., Li, D., Dansey, R. D., Godfrey, W. R., and Salles, G. A. (2014) PI3K $\delta$  inhibition by idelalisib in patients with relapsed indolent lymphoma. *N. Engl. J. Med.* **370**, 1008–1018
- Furman, R. R., Sharman, J. P., Coutre, S. E., Cheson, B. D., Pagel, J. M., Hillmen, P., Barrientos, J. C., Zelenetz, A. D., Kippes, T. J., Flinn, I., Ghia, P., Eradat, H., Ervin, T., Lamanna, N., Coiffier, B., Pettitt, A. R., Ma, S., Stilgenbauer, S., Cramer, P., Aiello, M., Johnson, D. M., Miller, L. L., Li, D., Jahn, T. M., Dansey, R. D., Hallek, M., and O'Brien, S. M. (2014) Idelalisib and rituximab in relapsed chronic lymphocytic leukemia. *N. Engl. J. Med.* **370**, 997–1007
- FDA (2014) FDA approves Zydelig for three types of blood cancers. Food and Drug Administration, Silver Spring, MD
- EMA (2014) Zydelig: summary of opinion (initial authorization). European Medicines Agency, London, UK
- Berndt, A., Miller, S., Williams, O., Le, D. D., Houseman, B. T., Pacold, J. I., Gorrec, F., Hon, W. C., Liu, Y., Rommel, C., Gaillard, P., Ruckle, T., Schwarz, M. K., Shokat, K. M., Shaw, J. P., and Williams, R. L. (2010) The p110  $\delta$  structure: mechanisms for selectivity and potency of new PI(3)K

## The Characterization of Idelalisib Binding to PI3K $\delta$

- inhibitors. *Nat. Chem. Biol.* **6**, 117–124
21. Fabian, M. A., Biggs, W. H., 3rd, Treiber, D. K., Atteridge, C. E., Azimioara, M. D., Benedetti, M. G., Carter, T. A., Ciceri, P., Edeen, P. T., Floyd, M., Ford, J. M., Galvin, M., Gerlach, J. L., Grotzfeld, R. M., Herrgard, S., Insko, D. E., Insko, M. A., Lai, A. G., Lélias, J. M., Mehta, S. A., Milanov, Z. V., Velasco, A. M., Wodicka, L. M., Patel, H. K., Zarrinkar, P. P., and Lockhart, D. J. (2005) A small molecule-kinase interaction map for clinical kinase inhibitors. *Nat. Biotechnol.* **23**, 329–336
  22. Copeland, R. A. (2000) Reversible inhibitors. In *Enzymes: A Practical Introduction to Structure, Mechanism, and Data Analysis*, pp. 266–304, A. John Wiley & Sons, Inc., New York
  23. Myszka, D. G., and Morton, T. A. (1998) CLAMP: a biosensor kinetic data analysis program. *Trends Biochem. Sci.* **23**, 149–150
  24. Myszka, D. G. (2000) Kinetic, equilibrium, and thermodynamic analysis of macromolecular interactions with BIACORE. *Methods Enzymol.* **323**, 325–340
  25. Myszka, D. G., He, X., Dembo, M., Morton, T. A., and Goldstein, B. (1998) Extending the range of rate constants available from BIACORE: interpreting mass transport-influenced binding data. *Biophys. J.* **75**, 583–594
  26. Karlsson, R. (1999) Affinity analysis of non-steady-state data obtained under mass transport limited conditions using BIACore technology. *J. Mol. Recognit.* **2**, 285–292
  27. Leslie, A. G. W., Powell, H. R. (2007) Processing diffraction data with MOSFLM, in *Evolving Methods for Macromolecular Crystallography* (Read, R. J., and Sussman, J. L., eds), pp. 41–51, Springer
  28. Evans, P. (2006) Scaling and assessment of data quality. *Acta Crystallogr. D Biol. Crystallogr.* **62**, 72–82
  29. Kissinger, C. R., Gehlhaar, D. K., and Fogel, D. B. (1999) Rapid automated molecular replacement by evolutionary search. *Acta Crystallogr. D Biol. Crystallogr.* **55**, 484–491
  30. Adams, P. D., Afonine, P. V., Bunkóczi, G., Chen, V. B., Davis, I. W., Echols, N., Headd, J. J., Hung, L. W., Kapral, G. J., Grosse-Kunstleve, R. W., McCoy, A. J., Moriarty, N. W., Oeffner, R., Read, R. J., Richardson, D. C., Richardson, J. S., Terwilliger, T. C., and Zwart, P. H. (2010) PHENIX: a comprehensive Python-based system for macromolecular structure solution. *Acta Crystallogr. D Biol. Crystallogr.* **66**, 213–221
  31. Emsley, P., Lohkamp, B., Scott, W. G., and Cowtan, K. (2010) Features and development of Coot. *Acta Crystallogr. D Biol. Crystallogr.* **66**, 486–501
  32. Wymann, M. P., Bulgarelli-Leva, G., Zvelebil, M. J., Piroola, L., Vanhaesebroeck, B., Waterfield, M. D., and Panayotou, G. (1996) Wortmannin inactivates phosphoinositide 3-kinase by covalent modification of Lys-802, a residue involved in the phosphate transfer reaction. *Mol. Cell. Biol.* **16**, 1722–1733
  33. Singh, J., Petter, R. C., Baillie, T. A., and Whitty, A. (2011) The resurgence of covalent drugs. *Nat. Rev. Drug Discov.* **10**, 307–317
  34. Sadhu, C., Masinovsky, B., Dick, K., Sowell, C. G., and Staunton, D. E. (2003) Essential role of phosphoinositide 3-kinase  $\delta$  in neutrophil directional movement. *J. Immunol.* **170**, 2647–2654
  35. Walker, E. H., Pacold, M. E., Perisic, O., Stephens, L., Hawkins, P. T., Wymann, M. P., and Williams, R. L. (2000) Structural determinants of phosphoinositide 3-kinase inhibition by wortmannin, LY294002, quercetin, myricetin, and staurosporine. *Mol. Cell* **6**, 909–919
  36. Cushing, T. D., Hao, X., Shin, Y., Andrews, K., Brown, M., Cardozo, M., Chen, Y., Duquette, J., Fisher, B., Gonzalez-Lopez de Turiso, F., He, X., Henne, K. R., Hu, Y. L., Hungate, R., Johnson, M. G., Kelly, R. C., Lucas, B., McCarter, J. D., McGee, L. R., Medina, J. C., San Miguel, T., Mohn, D., Pattaropong, V., Pettus, L. H., Reichelt, A., Rzasca, R. M., Seganish, J., Tasker, A. S., Wahl, R. C., Wannberg, S., Whittington, D. A., Whoriskey, J., Yu, G., Zalameda, L., Zhang, D., and Metz, D. P. (2015) Discovery and in vivo evaluation of (S)-N-(1-(7-fluoro-2-(pyridin-2-yl)quinolin-3-yl)ethyl)-9H-purin-6-amine (AMG319) and related PI3K $\delta$  inhibitors for inflammation and autoimmune disease. *J. Med. Chem.* **58**, 480–511
  37. Knight, Z. A., Gonzalez, B., Feldman, M. E., Zunder, E. R., Goldenberg, D. D., Williams, O., Loewith, R., Stokoe, D., Balla, A., Toth, B., Balla, T., Weiss, W. A., Williams, R. L., and Shokat, K. M. (2006) A pharmacological map of the PI3-K family defines a role for p110 $\alpha$  in insulin signaling. *Cell* **125**, 733–747